



**HAL**  
open science

## A wireless motion sensor operating down to -28dBm energy harvesting

Yero Dia, Helena Ribeiro, Laurent Oyhenart, Elie Zaraket, Ludivine Fadel, Valerie Vigneras, Corinne Dejous, Nuno Carvalho, Simon Hemour

► **To cite this version:**

Yero Dia, Helena Ribeiro, Laurent Oyhenart, Elie Zaraket, Ludivine Fadel, et al.. A wireless motion sensor operating down to -28dBm energy harvesting. *IEEE Journal of Radio Frequency Identification*, 2024, pp.1-1. 10.1109/JRFID.2024.3374648 . hal-04559986

**HAL Id: hal-04559986**

**<https://hal.science/hal-04559986v1>**

Submitted on 26 Apr 2024

**HAL** is a multi-disciplinary open access archive for the deposit and dissemination of scientific research documents, whether they are published or not. The documents may come from teaching and research institutions in France or abroad, or from public or private research centers.

L'archive ouverte pluridisciplinaire **HAL**, est destinée au dépôt et à la diffusion de documents scientifiques de niveau recherche, publiés ou non, émanant des établissements d'enseignement et de recherche français ou étrangers, des laboratoires publics ou privés.

# A wireless motion sensor operating down to -28dBm energy harvesting

Yero Dia, *Student Member, IEEE*, Helena Ribeiro, *Student Member, IEEE*, Laurent Oyhenart, Elie Zaraket, *Student Member, IEEE*, Ludivine Fadel, Valerie Vigneras, Corinne Dejous, *Member, IEEE*, Nuno Carvalho, *Fellow, IEEE*, and Simon Hemour, *Senior Member, IEEE*

**Abstract**—ZeroPower devices are the next generation of Internet of Things. Typically tapping from ambient energy, or activated by a remote reader, their first and foremost challenge is the operation distance from the nearest RF source. Unfortunately, these systems can only be activated within a range of a few tens of meters due to their minimum activation power (also named reading sensitivity). This work reduces the harvesting power to a new threshold of -28dBm (1.5  $\mu$ W). We demonstrate a wireless motion sensor operating in burst mode with as low as 120 mV of DC voltage and 0.72  $\mu$ J of stored energy. This efficient operation is achieved without any DC/DC conversion thanks to a four-stages rectifier biasing a tunnel diode Voltage-controlled oscillator (VCO).

**Index Terms**—RFID, ZeroPower, ambient power, transponder, tunnel diode, rectifier, energy harvesting, backscattering.

## I. INTRODUCTION

The Fourth Industrial Revolution, often called Industry 4.0, describes the present stage of industrialization that merges the physical and digital worlds. It entails a novel approach to manufacturing processes by integrating virtual and real-world elements. This new industry blends digital design and engineering with physical products and systems [1].

Industry 4.0 is based on the Internet of Things (IoT), which has enabled the connection of sensor networks and their market deployment. In 2019, the number of these connected devices was estimated at 34 billion and is projected to reach \$93.86 billion by 2023 [2]. Also, it is widely recognized that radio transmission of those wireless devices in embedded systems is the most energy-consuming part of the energy budget [3]. Although low-power communication protocols exist (such as Bluetooth Low Energy or Zigbee), they are often integrated into transmitters that consume at least twenty milliwatts [4]. Thus, energy efficiency remains a crucial consideration for wireless sensor nodes (WSN) [5], as decreasing the energy used for communication can appreciably enhance the longevity of wireless sensor nodes.

Recent advancements have provided viable solutions to overcome the challenges of energy efficiency in sensor networks, including the development of more compact and

energy-efficient networks. A notable approach involves duty-cycling the radio, wherein the transmitter periodically switches between active and inactive states to lower power usage [6]. However, this method still incurs power consumption during idle periods. A more sophisticated alternative is backscattering communication, which offloads the wireless communication energy cost to the reader device.

Originating in the late 1940s [7], this approach enables a transponder to reflect data when illuminated by a reader signal. Radio Frequency Identification (RFID) technology, which leverages this principle, uses RF wave energy to both transmit data to the tag and power the transmission circuit. Despite its low power consumption (Fig. 1a), RFID needs continuous power supply from a nearby system for operation.

Many attempts have been made to enhance the distance between the RFID tag and the power source, and one popular method is to incorporate a repeater structure between the reader and the tag [8], [9]. However, it should be noted that this approach is not entirely passive due to the energy consumption associated with amplification. Moreover, a potential approach to improve range capabilities is by implementing bistatic systems, which involve physically separating the carrier emitter and the backscatter receiver. This separation enables an extended range, although it necessitates an additional energy source to power the second antenna [10], [11].

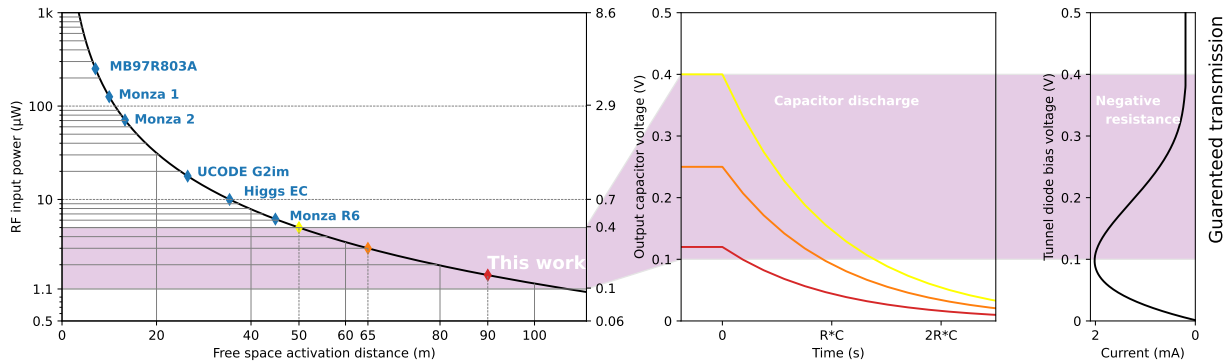
The advent of ambient backscattering introduces the potential to eliminate the dependency of RFID tag being near a power source [12]–[14]. By harnessing energy from ambient RF waves, it becomes feasible to operate over larger areas without direct power sources. Maximizing this technology's efficiency requires integrating an energy-harvesting system with an ultra-low voltage transmitter, potentially utilizing a tunnel diode [15] known for its negative resistance feature (Fig. 1a). In addition, incorporating this component offers a practical resolution for reducing power consumption in wireless transceivers by eliminating the need for power amplifier and RF synthesizing circuitry, which are the primary power-consuming elements in the budget link. The implementation of such a system can greatly contribute to minimizing the losses incurred due to tool disappearance within the industrial environment.

Indeed, in aviation, the pervasive issue of foreign object damage (FOD) has posed a significant risk for an extensive period. This problem has resulted in catastrophic incidents and fatalities, contributing to an exorbitant cost of approximately \$4 billion annually [16]. To address this challenge, we propose

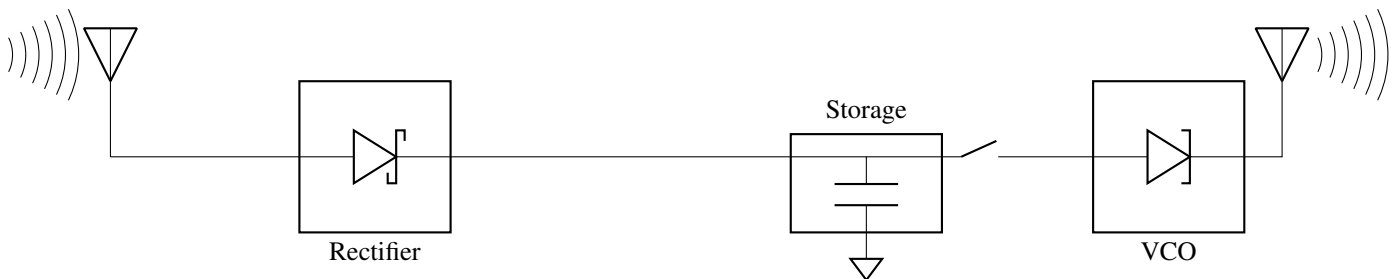
Manuscript received April 19, 2021; revised August 16, 2021. *Corresponding author: Yero Dia*

Yero Dia, Laurent Oyhenart, Elie Zaraket, Ludivine Fadel, Valerie Vigneras, Corinne Dejous, and Simon Hemour are with the Laboratoire IMS, Université de Bordeaux, 33400 Talence, France (e-mail:yero.dia@u-bordeaux.fr).

Helena Ribeiro, and Nuno Carvalho are with the Instituto de Telecomunicações, Universidade de Aveiro, Aveiro, Portugal.



(a) **(Left graph)** Theoretical free space activation distance of few industrial RFID tags: using their read sensitivity and Friis equation with a 36 dBm EIRP source at 956 MHz with a transmitter antenna gain of 5 dB and a receiver antenna gain of 2 dB. **(Middle graph)** Upon triggering, a capacitance can be discharged into a tunnel diode, yielding Frequency-Modulated Continuous Wave (FMCW) signal. **(Right graph)** I(V) characteristic of the tunnel diode. Purple area correspond to negative differential resistance region, where oscillation condition can be found.



(b) Architecture of the proposed system: a rectifier based on Schottky diode will convert radiofrequency waves from an antenna into DC voltage in a storage capacitor. Then a tunnel diode VCO will lead to emission of radiofrequency waves when oscillation criteria are reached.

Fig. 1: Performance of few industrial RFID tags and architecture of the proposed system.

a battery-less connected tag that can be attached to tools, mobile equipment, or products to facilitate their location upon movement through the use of a motion sensor.

Various approaches have been suggested in the existing literature to tackle the problem of minimal power activation, including the utilization of fully passive components or the enhancement of signal reception by the reader [15], [17]–[19]. Nevertheless, none of the solutions discussed in the literature have ventured into reducing power sensitivity through modifications to the rectifier side of the system that could help to reduce significantly the power of activation.

In our previous study [20], we briefly introduced an ambient backscattering system utilizing a voltage-controlled oscillator with a tunnel diode. In this extended edition of our research, we strive to explore deeper into the energy harvesting system by presenting a comprehensive analysis and an elaborated model of the complete system.

The paper is structured as follows: the initial section will introduce the rectifier used for RF to DC power conversion. The second section will present the voltage-controlled oscillator circuit and the construction of the simulation model. Lastly, we will discuss the constructed test bench and the obtained results.

## II. RECTIFIER

Radiofrequency energy harvesting can be utilized to power a system thanks to a rectenna [21]. Thus, through an antenna, the RF waves produced by the surrounding communicating systems are captured and converted through an RF to DC conversion circuit, the rectifier.

In this work, the node will be powered by an external source to highlight the proof of concept.

Rectifier circuits allow for the conversion of an RF signal into a DC signal. However, at the working frequencies (around 900 MHz), these circuits see their input impedance change depending on the input power, frequency, and also the load. Likewise, there are numerous topologies to maximize the output voltage or its efficiency.

This section will present the design choices and characterization of the rectifier used to operate in the GSM band and power the oscillator presented in the following section.

### A. Matching network

The input impedance of the rectifier, mostly capacitive has to be matched to the 50 Ω output impedance of the antenna.

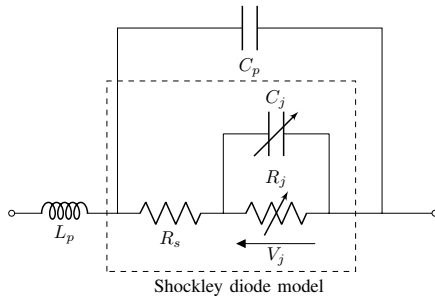
Thus, a L-matching circuit is used combining a discrete component followed by a shunt short-circuited distributed

component (stub) as at microwaves frequencies, the parasitic components contained inside lumped elements becomes more and more perceptible [22].

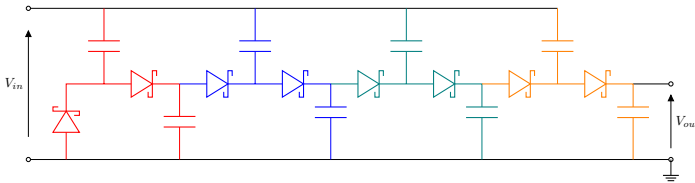
Moreover, a degree of liberty is lost also since those lumped components are available for discrete values. A final advantage of having a mix of discrete and distributed components for impedance match is the ability to tune the circuit after being manufactured.

### B. Topology

In literature, various rectifier topologies can be found, however, voltage multipliers are deemed the most preferable option for RF to DC rectification due to their straightforward design and its ability to answer to the target voltage requirement. Mathematically, the output voltage of a voltage doubler is  $V_{out} = 2V_{in} - 2V_j$  where  $V_j$  corresponds to the junction voltage of the diode used (Fig. 2a).



(a)



(b)

Fig. 2: (a) Shockley model of a packaged Schottky diode and (b) Improved voltage doubler topology for RF rectification:  $100\text{ pF}$  capacitors are connected to the input while  $100\text{ nF}$  are connected to the ground.

In traditional low frequency (LF) rectifiers, multiple stages of voltage multiplication are often connected in series to boost the output voltage. However, this approach can cause significant power loss in RF rectifiers due to the high frequency signals involved. This is because at RF frequencies, the capacitors used in voltage multiplication stages can act as inductive loads, leading to undesirable reflections and resonances. These effects can result in signal distortion, reduced efficiency, and increased losses in the rectifier. Therefore, alternative approaches are required to address these challenges in RF rectification [23].

Therefore, it is more advisable to utilize an alternative topology wherein the rectifier stages are cascaded in a pseudo series-parallel arrangement. In this configuration, the outputs of the rectifiers are linked in series (daisy-chained), while their inputs remain in parallel with the RF input. By employing this

technique, it is also possible to apply it to the voltage doubler rectifier, resulting in the creation of multiple stages (Fig. 2b).

### C. Diode choice

Choosing the appropriate diode is a critical aspect in the design of a rectifier for low power energy harvesting situations. The efficiency of rectification is greatly influenced by this selection process. Schottky diodes are frequently preferred for RF to DC conversion because they possess a low barrier voltage ( $V_j$ ), which makes them suitable for such applications [24].

The conversion is done through the bias of the capacitance and junction resistance of the Shockley model of the diode. The resistance  $R_s$  represents the losses of the diode and  $C_p$  and  $L_p$  are packaging capacitance and inductance. The lower the impedance of the resistance and junction capacitance, the less they will hinder the conversion. Additionally, when an RF current flows through the junction, the capacitance  $C_j$  will draw more current if its impedance is lower than that of the junction resistance, although ideally it should pass through the non-linear junction resistance  $R_j$ .

To summarize, the impedance of the junction capacitance ( $C_j$ ) should be lower than the resistance of the junction ( $R_j$ ) to draw more RF current. Both  $C_j$  and  $R_s$  should be chosen as low as possible to minimize their impeding effects and improve the rectifying operation [25].

Parameter	Unit	HSMS-285x	SMS-7630
$B_v$	V	3.8	2
$C_{J0}$	pF	0.18	0.14
$E_G$	eV	0.69	0.69
$I_{Bv}$	A	$3e-4$	$1e-4$
$I_S$	A	$3e-6$	$5e-6$
N		1.06	1.05
$R_S$	$\Omega$	25	20
$P_B (V_j)$	V	0.35	0.34
$P_T (XTI)$		2	2
M		0.5	0.4

TABLE I: Datasheet of two Schottky diode in radiofrequency energy harvesting.

This study aimed to identify the optimal choice between two diodes, specifically the HSMS-2850 and SMS-7630. The junction potentials of these diodes were measured to be 0.35 V and 0.34 V, while their breakdown voltages were recorded as 3.8 V and 2 V respectively (Table I). Full wave rectifiers were constructed using these diodes in order to rectify at 900 MHz and measure their sensitivity. The results (Fig. 3) clearly indicated that the sensitivity is dependent on the input power, with superior results observed for the HSMS-2850 diode. In other works, the first diode was chosen because it shows the best results for power conversion efficiency at low power [26], [27].

After choosing the diode to be used, it is important to determine the number of stages. It is reminded that the goal is to have a sufficiently high voltage for very low power supplies.

Increasing the number of stages in a circuit beyond four may lead to a decrease in output voltage due to the additional complexity and associated losses incurred during signal propagation. This can result in a decrease in overall circuit

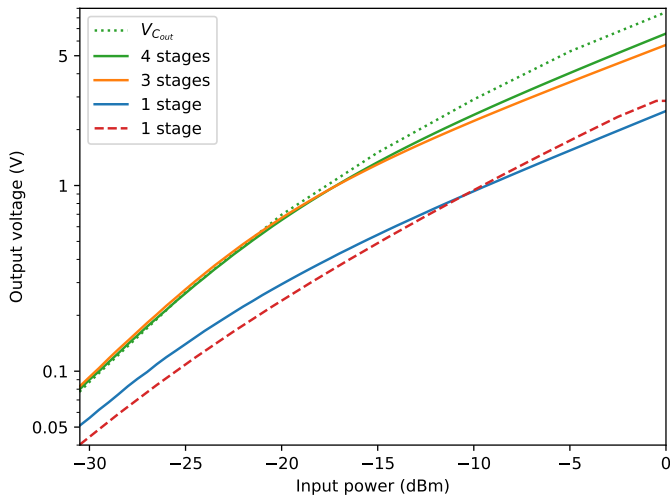


Fig. 3: Output voltage of different stages vs. Input power: *the solid and dotted line curves use the HSMS2850 diode while the dashed curve uses the SMS 7630 diode.*

efficiency and output power [28]. Indeed, as presented in our previous studies, adding a stage thus improves sensitivity to low power levels but reduces efficiency for the same load [29], [30]. However, a similar efficiency is achieved at a higher load since the optimal load corresponds to the sum of all the diode junction resistances at low power levels and decreases as the input power increases. As shown in Fig. 3, the output voltages of a 3-stage and a 4-stage rectifier converge. Also, previous studies have been conducted to select a 4-stage rectifier that allows for obtaining the highest possible voltage for low powers [30], [31]. At -30 dBm, the optimal load found is around 60 k $\Omega$ .

#### D. Characterization

In the case of the low-power RF harvester, the energy is stored in a capacitor or other storage element for later use by the application. This accumulation mode prioritizes power sensitivity over power efficiency during the charging process. During characterization, the rectifier is disconnected from the load, which represents the equivalent impedance of the actual application being powered. This allows for a more precise measurement and analysis of the harvester's performance in this specific mode of operation.

The rectifier is produced using mechanical engraving on a FR-4 printed circuit board, which has a relative permittivity  $\epsilon_r$  of 4.7 and a loss tangent  $\tan(\delta)$  of 0.014. The board has a thickness of 1.6 mm and is coated with 35  $\mu\text{m}$  of copper.

The blue curve in Fig. 4 represents the anticipated DC voltage at the rectifier output for an input power of -28 dBm in the GSM downlink frequency band. This is demonstrated in red in Fig. 4, which also shows the superposition of the return loss at the same power level. It is noticeable that the maximum voltage peak coincides with the frequency at which the return loss is minimum. As a result, the operating frequency of the rectifier will be 949 MHz, which will provide the highest voltage output for low input power. Nevertheless,

measurements of output voltage and reflection coefficient present a close form response with respect to the simulation results with a shift of around 20 MHz mainly due to fabrication issues.

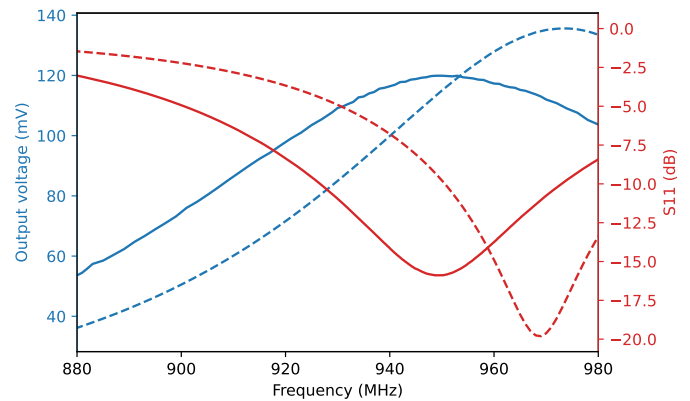


Fig. 4: Rectenna frequency characterization at -28.6dBm: **(blue)** Measured return loss S11 of the 4-stages rectifier. **(red)** Measured output voltage of the 4-stage rectifier at 949 MHz. *Solid lines curves are experimental results while dashed one are simulation results.*

Batteries are utilized for sensors that require a significant amount of power, ranging from milliwatts to several hundred milliwatts. However, one drawback of these devices is that their capacity deteriorates after a few thousand cycles [32].

On the other hand, capacitors possess a capacity that can support numerous charge cycles [33]. Additionally, their low power density enables them to charge at a faster rate compared to batteries.

Consequently, a capacitor can be employed to store and release charges once a certain threshold is reached. To evaluate this, a 100  $\mu\text{F}$  capacitor is added to the output of the rectenna and subjected to characterization. The rectifier is a novel time characterized at 949 MHz, with an input power ranging from -30 dBm to 0 dBm (Fig. 3, green dots).

### III. VOLTAGE CONTROLLED OSCILLATOR (VCO)

There are two types of oscillators commonly used: ring type and LC type oscillators. Ring type oscillators utilize CMOS technology and employ NOT gates arranged in a ring configuration. On the other hand, LC type oscillators generate oscillations using parasitic components within the circuits. Previous studies such as [34], [35] have shown the use of ring type oscillators in various applications. However, LC type oscillators offer advantages such as lower fabrication cost and a reduced bias voltage limitation.

While Power Amplifiers (PAs) are widely favored for radiofrequency transmission due to their high efficiency, they do have a significant drawback. The activation requirement for PAs is relatively high, typically greater than 0.4 V [36]–[39]. This is due to the threshold voltage of the transistor, which is limited compared to the low voltage capabilities of tunnel diode oscillators. In an ambient RF energy harvesting scenario [40], the low power levels (as shown in Figure 1a, left) may

result in insufficient voltage conversion to adequately power a power amplifier (PA).

In this project, the focus will be on LC type oscillators using readily available lumped components. This approach aims to lower the fabrication cost and overcome the bias voltage limitation associated with PA. By exploring the potential of LC type oscillators, this research aims to contribute to the improvement of oscillator technologies for various scientific applications.

### A. Principle of a VCO

When considering electrical components (Fig. 5), a system will begin oscillating at a frequency  $f$  only if there is a negative sum of resistances ( $R_l$  and  $R_{in}$ ) and a zero sum of reactance ( $X_{in} = X_L$ ) due to transient excitation or noise. This occurs when loss is balanced by gain, as stated by the Barkhausen criterion for energy generation [41], [42].

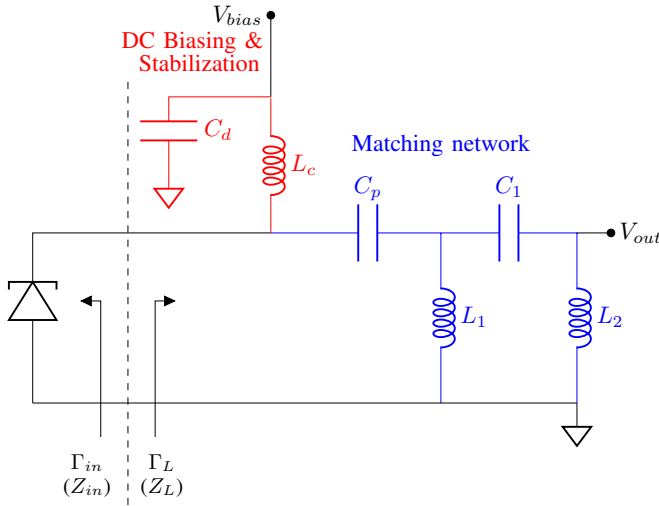


Fig. 5: Schematic of the tunnel diode voltage controlled oscillator.

The operating principle of a Voltage-Controlled Oscillator (VCO) is based on the phenomenon that the frequency output of an oscillator can be controlled by varying an input voltage. When a varying control voltage is applied, it modulates the capacitance or resistance of the voltage-sensitive element, which in turn alters the resonant frequency of the tank circuit. This modification of the resonant frequency directly proportional to the control voltage leads to a variation in the output frequency of the VCO.

### B. VCO circuit design

Tunnel diodes present inherent properties for voltage controlled oscillators (VCOs): on the one hand, they exhibit negative differential resistance (which leads to instability potential [42]) when correctly biased, and on the other hand, their junction capacitance and junction resistance vary significantly with the applied voltage, which improves the VCO sensitivity. The oscillation conditions are relatively simple and are fulfilled when the total circuit equivalent resistance becomes zero.

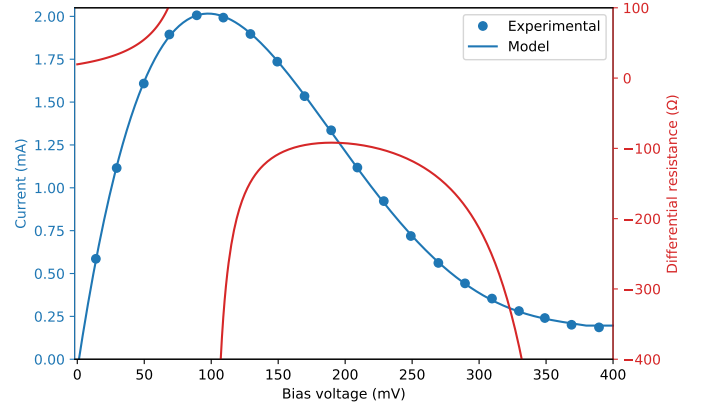


Fig. 6: Measured and modeled tunnel diode's IV characteristic with its negative differential resistance.

Before creating a prototype using a tunnel diode, it is essential to determine the direct current (DC) voltage and current (IV) relationship of the tunnel diode. The N-type gallium-arsenide (Ga-As) tunnel diode, model 3I306E, is selected and its current-voltage (I-V) characteristic is measured. In the voltage range of 120 mV to 450 mV, the current decreases, which corresponds to the region of negative dynamic resistance as depicted in Fig. 6.

### C. Simulation framework

The VCO frontend can be seen in Fig. 5 and comprises a tunnel diode, a DC biasing and stabilization network, and a matching network as presented in [20], [43].

To improve the precision of the simulation performance, it is important to extract a model of the tunnel diode. The diode's S-parameters and IV curves were extracted using a PNA-X and a power analyzer to achieve this. The acquired values were subsequently employed to model the charge equation and IV curve accurately through polynomial fitting.

The use of an equation-based model in Advance Design System (ADS) allows for the study of a tunnel diode as a nonlinear component using the symbolically defined device (SDD).

This model can accurately simulate the behavior of the device, both for small signals and large signals, without the need for source code. A 7th order polynomial equation (1),  $I(v)$ , is specifically utilized to accurately simulate the DC or harmonic balance simulation of a tunnel diode [44]:

$$I(v) = \begin{cases} 10^{-12}(\exp^{\frac{v-0.2}{26 \times 10^{-3}}} - 1) + 1.96e - 4 & \text{if } v > 0.38 \\ A + Bv + Cv^2 + Dv^3 + Ev^4 + Fv^5 + Gv^6 + Hv^7 & \text{else.} \end{cases} \quad (1)$$

The charge curve is needed for the tunnel diode model because it provides information about the behavior of the diode at different levels of applied voltage.

The charge curve shows the relationship between the voltage applied to the diode and the amount of charge stored within it (Equation 2). This relationship is crucial for understanding



how the tunnel diode behaves at different voltages, as it determines the point at which the negative resistance occurs.

$$Q(v) = \begin{cases} 9 \times v - 0.28 \times 10^{-12} & \text{if } v > 0.35 \\ 0 & \text{if } v < 0 \\ v(A + Bv + Cv^2 + Dv^3 + Ev^4 + Fv^5 + Gv^6 + Hv^7) & \text{else.} \end{cases} \quad (2)$$

The various values of the equations for the characteristics  $I(v)$  and  $Q(v)$  are compiled in Table II.

TABLE II: Parameters of the Polynomial in the  $I(v)$  and  $Q(v)$  curves.

Parameter	Value for $I(v)$	Value for $Q(v)$
A	-6.31e-5	6.2e-12
B	0.05	3.6e-11
C	-0.41	-6.3e-10
D	1.11	6.55e-9
E	-0.55	-3.93e-8
F	-3.22	1.36e-7
G	7.46	-2.47e-7
H	-5.75	1.84e-7

The parasitic element of this tunnel diode can be simplified as a 2.09 nH inductor with a diode serie resistance of 1.5 Ohm. The SDD block from ADS was used to simulate the behavior of a tunnel diode. The final model of the tunnel diode can be seen in Fig. 7.

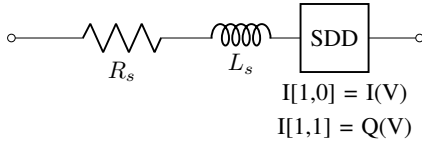


Fig. 7: Tunnel diode model using the Symbolically-Defined Device (SDD) in Keysight ADS. The first equation  $I[1,0]$  refers to the current flowing through the port 1 of the device, i.e.  $I(t)=I(v(t))$ , using the equation 1. The second equation  $I[1,1]$  refers to the current flowing through the port 1 of the device with time differentiation in the time domain, i.e.  $I(t)=\frac{d}{dt}Q(v(t))$ .

A transient simulation of the tunnel diode using the SDD block is able to reproduce the experimental results obtained during the discharging of the output capacitance of the rectifier (Fig. 8, right). The results show two different regimes, appearing with two different slopes. Below 380 mV, the tunnel diode exhibits negative resistance, leading to oscillations, current demand, and voltage drop. It is within this range that the oscillations can be observed, as shown in Fig. 1a. Also, as seen in Fig. 8, left, the wireless sensor needs 20 seconds of harvesting time (under -28dBm exposure) to reach the 720nJ necessary to transmit a burst, while it takes only around 1 second under -22 dBm RF harvesting power.

The oscillation frequency range of the designed circuit is influenced by its DC Biasing and Stabilization network. The oscillation frequency can be actively adjusted by varying the DC bias between 0.15 V and 0.33 V. To achieve the desired oscillation frequency,  $L_c$  and  $C_d$  have been set to 10 nH and

1 nF, respectively. The matching network consists of two 10 nH inductors and a 4 pF capacitor. In Fig. 6, it is possible to observe that the signal generated by the VCO does really appear on the negative differential resistance part.

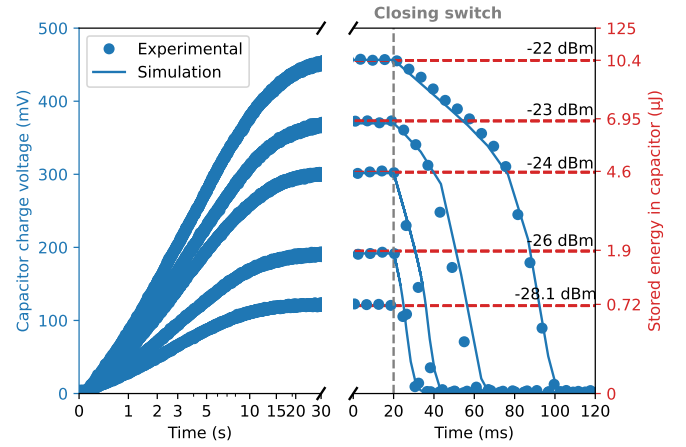


Fig. 8: Experimental discharges of the 100 $\mu$ F capacitor into the tunnel diode and its simulation.

## IV. MEASUREMENTS AND DISCUSSION

### A. Test bench

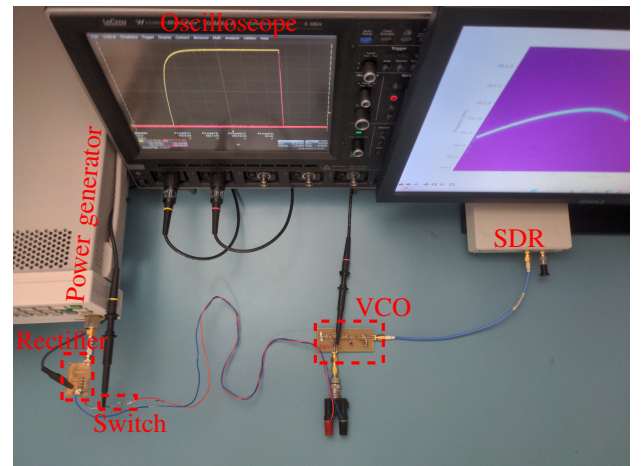


Fig. 9: Experimental bench designed for the measurements: the power generator (Keysight/Agilent N5182A) powers the rectifier presented in section II. A tilt switch will allow the rectifier to bias the tunnel bias VCO presented in section III. Output frequency is measured thanks to a radio receiver (NI USRP 2901) and voltage thanks to an oscilloscope (Lecroy 104MXs-A).

As part of the system validation, the Voltage-Controlled Oscillator (VCO) is powered by the output of a RF-to-DC converter (rectifier) to demonstrate the system concept. In contrast to amplifiers and most 2-ports microwave devices/circuits, oscillators and generators just have one RF (output) port. However, it is interesting to observe the DC biasing (DC link from the rectifier to the oscillator), given in Fig. 8. Also,

in a power transmission application, the rectifier would be connected to an antenna operating in the GSM frequency band. However, the focus is on demonstrating the system concept. To accomplish this, a Keysight/Agilent N5182A power generator is used to power the rectifier.

Similarly, a NI USRP 2901 radio receiver is connected to the output of the VCO to measure the frequency and power of the generated output signal. The measurements will be performed using the open-source software GNU Radio and processed digitally using Python.

To initiate the discharge of the capacitor in the VCO circuit, a tilt switch, which is sensitive to movement is placed between the subsystems. Moving it will cause the switch to close and the oscillation to start.

Finally, a Lecroy 104MXs-A oscilloscope is used to measure the voltage across the capacitor and at the entrance of the VCO circuit. Fig. 9 presents the whole test bench.

**B. Characterization**

In our experimental setup, the input power to the rectifier is adjusted to replicate the level that can be obtained in an urban environment [40]. We then measure the output voltage of the rectifier and plot the frequency as a function of it (Fig. 10). Our results demonstrate that a minimum input power of around -28 dBm is necessary to generate a high-frequency signal.

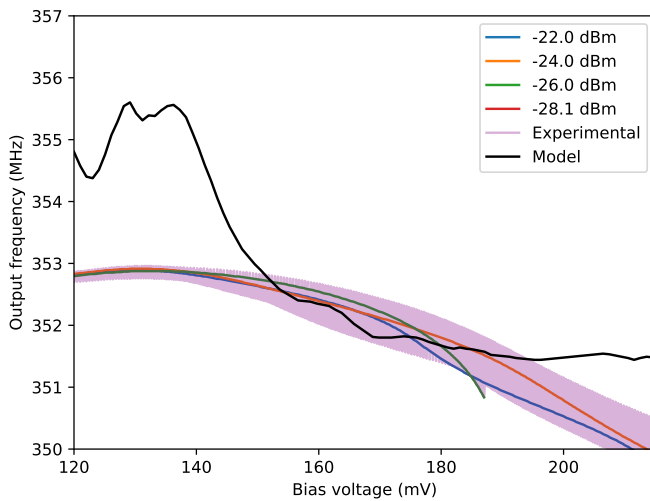


Fig. 10: Output frequency of the generated signal: *solid lines are experimental results and dashed one is simulation. The purple "experimental" zone corresponds to the upper and lower limits of a set of 18 experimentally measured curves, which are not displayed here.*

The oscillation frequency is shown in Fig. 10. As the voltage stored in the capacitor is decreasing over time, the tunnel diode circuit is biased by a swept voltage. Since a variant junction capacitance and negative differential resistance correspond to every bias voltage, the conditions of oscillations and generated frequency varies accordingly. The experimental values are compared to simulation, according to the methodology described in [45]. The simulation modeling involves the derivation of measurement data. This turns into

significant challenges when attempting to accurately model the high resistance corresponding to the Tunnel diode peak's current. We acknowledge increased modeling uncertainties in this region. This is also attributed to the utilization of a 50 Ohm Vector Network Analyzer (VNA) for diode characterization: while a VNA is proficient in accurately measuring impedances of around 50 ohms, it is not ideal for measuring resistances in the magnitude of thousands of ohms.

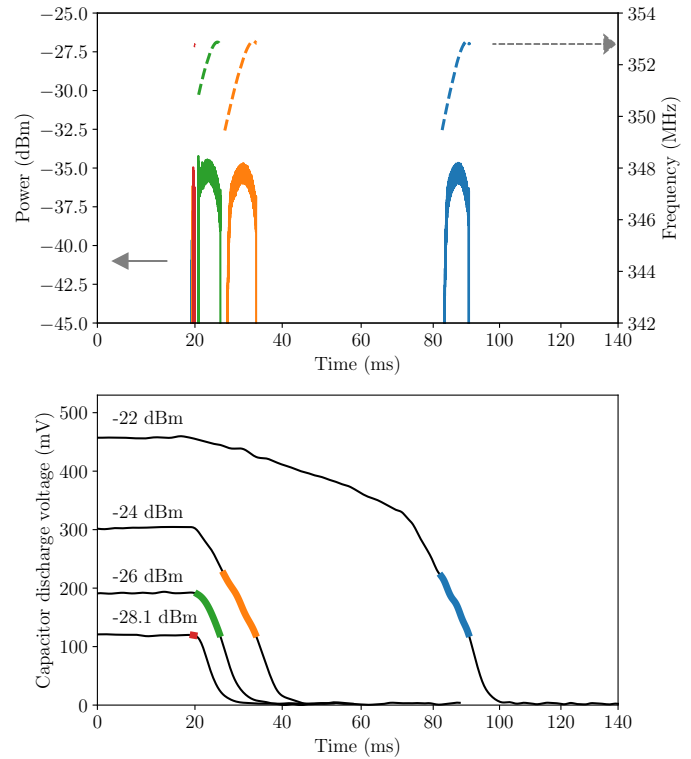


Fig. 11: Transient results of the constructed VCO. *Top: generated chirp by the system and output power of the generated signal. Bottom: Discharging capacitor into the VCO circuit, in solid colored line, the generated oscillation.*

These changes in capacitance and resistance lead to a decrease in the oscillation frequency. An increased junction capacitance causes the overall resonant frequency of the circuit to decrease, as the capacitive reactance becomes larger. This results in a lower frequency of oscillation for a given resonant circuit. Similarly, an increased junction resistance dampens the oscillation, causing the frequency to decrease even further. This phenomenon is known as the "degeneration" of the oscillator, which occurs as a result of the increased junction capacitance and resistance [46].

Finally, after calibrating the USRP, the power of the high-frequency output signal is determined (Fig. 11-top). This measurement demonstrates that the system implemented is resilient to the input power of the system and will be able to generate a sufficiently powerful signal for transmission via a 50 Ω antenna.

Similarly, the oscillation time is approximately 8 milliseconds. However, when the polarization voltage is below 220 milliseconds, the oscillation time reduces further (Fig. 11-top).



TABLE III: Performance comparison

Ref	$F_{in}$	$F_{out}$	$P_{min}$	$d_{act}$	$V_{min}$
[15], 2020	900 MHz	5.8 GHz	-5 dBm	6.64 m	88 mV
[17], 2020	865-868 MHz band	4 GHz	-13 dBm	17.37 m	NA
[18], 2019	5.8 GHz	5.8 GHz	-16.7 dBm	3.97 m	80 mV
[19], 2017	5.8 GHz	5.8 GHz	-16.9 dBm	4.06 m	NA
<b>This work</b>	<b>900 MHz band</b>	<b>350 MHz</b>	<b>-28 dBm</b>	<b>90.1 m</b>	<b>120 mV</b>

Table III facilitates the comparison of this work with other research papers showing that the system designed generates the signal with the lowest power at the input of the rectifier circuit. This is due to the fact that all the components are off-the-shelf (COTS) components requiring no external power supply. Also, the theoretical free space activation distance is computed allowing to understand how far the system can be from the source.

The calculation is made using Friis equation with 6 dBm EIRP source at their working input frequency and power activation, with a transmitter antenna gain of 5 dB and a receiver antenna gain of 2 dB.

## V. CONCLUSION AND FUTURE WORKS

This work describes the design and measurements of a RFID tag with very low reading sensitivity. This system revolves around a tunnel diode that creates oscillation through its negative resistance, all powered by a rectifier that can utilize ambient energy harvesting. The presented tag operates at power levels on the order of microwatts (-28 dBm) and is capable of outputting an oscillating signal at -35 dBm. Such an application is particularly interesting for low RF power environments such as inside factories and buildings.

The built system can still be improved by adding antennas at the input and output of the assembly. Similarly, by adding a diplexer, the system can become more compact by having a single antenna that allows both energy conversion and signal transmission.

## ACKNOWLEDGEMENT

The author wish to thank Pablo Pérez-Nicoli and Jean-Luc Lachaud for fruitful discussions.

## REFERENCES

- [1] J. Wan, H. Cai, and K. Zhou, "Industrie 4.0: enabling technologies," in *Proceedings of 2015 international conference on intelligent computing and internet of things*. IEEE, 2015, pp. 135–140.
- [2] D. Catenazzo, B. O'Flynn, and M. Walsh, "On the use of wireless sensor networks in preventative maintenance for industry 4.0," in *2018 12th International Conference on Sensing Technology (ICST)*. IEEE, 2018, pp. 256–262.
- [3] M. H. Alsharif, S. Kim, and N. Kuruoğlu, "Energy harvesting techniques for wireless sensor networks/radio-frequency identification: A review," *Symmetry*, vol. 11, no. 7, p. 865, 2019.
- [4] "CC2651R3SIPA datasheet," Texas Instruments, Texas, USA.
- [5] N. R. Patel and S. Kumar, "Wireless sensor networks' challenges and future prospects," in *2018 International Conference on System Modeling & Advancement in Research Trends (SMART)*. IEEE, 2018, pp. 60–65.
- [6] D. Passos, H. Balbi, R. Carrano, and C. Albuquerque, "Asynchronous radio duty cycling for green iot: State of the art and future perspectives," *IEEE Communications Magazine*, vol. 57, no. 9, pp. 106–111, 2019.
- [7] H. Stockman, "Communication by means of reflected power," *Proceedings of the IRE*, vol. 36, no. 10, pp. 1196–1204, 1948.
- [8] S. Sabesan, M. Crisp, R. V. Penty, and I. H. White, "Passive uhf rfid interrogation system using wireless rfid repeater nodes," in *2013 IEEE International Conference on RFID (RFID)*. IEEE, 2013, pp. 136–143.
- [9] A. G. Dimitriou, "Design, analysis, and performance evaluation of a uhf rfid forward-link repeater," *IEEE Journal of Radio Frequency Identification*, vol. 4, no. 2, pp. 73–82, 2019.
- [10] J. Kimionis, A. Bletsas, and J. N. Sahalos, "Increased range bistatic scatter radio," *IEEE Transactions on Communications*, vol. 62, no. 3, pp. 1091–1104, 2014.
- [11] B. S. Ciftler, A. Kadri, and I. Güvenç, "Tot localization for bistatic passive uhf rfid systems with 3-d radiation pattern," *IEEE Internet of Things Journal*, vol. 4, no. 4, pp. 905–916, 2017.
- [12] V. Liu, A. Parks, V. Talla, S. Gollakota, D. Wetherall, and J. R. Smith, "Ambient backscatter: Wireless communication out of thin air," *ACM SIGCOMM computer communication review*, vol. 43, no. 4, pp. 39–50, 2013.
- [13] N. Van Huynh, D. T. Hoang, X. Lu, D. Niyato, P. Wang, and D. I. Kim, "Ambient backscatter communications: A contemporary survey," *IEEE Communications surveys & tutorials*, vol. 20, no. 4, pp. 2889–2922, 2018.
- [14] V. Palazzi, R. Correia, X. Gu, S. Hemour, K. Wu, A. Costanzo, D. Masotti, E. Fazzini, A. Georgiadis, H. Kazemi *et al.*, "Radiative wireless power transfer: Where we are and where we want to go," *IEEE Microwave Magazine*, vol. 24, no. 2, pp. 57–79, 2023.
- [15] A. Eid, J. Hester, and M. M. Tentzeris, "A 5.8 ghz fully-tunnel-diodes-based 20  $\mu$ w, 88mv, and 48 db-gain fully-passive backscattering rfid tag," in *2020 IEEE/MTT-S International Microwave Symposium (IMS)*. IEEE, 2020, pp. 607–610.
- [16] T. Chauhan, C. Goyal, D. Kumari, and A. K. Thakur, "A review on foreign object debris/damage (fod) and its effects on aviation industry," *Materials Today: Proceedings*, vol. 33, pp. 4336–4339, 2020.
- [17] D. Dardari, N. Decarli, A. Guerra, M. Fantuzzi, D. Masotti, A. Costanzo, D. Fabbri, A. Romani, M. Drouguet, T. Feuillen *et al.*, "An ultra-low power ultra-wide bandwidth positioning system," *IEEE Journal of Radio Frequency Identification*, vol. 4, no. 4, pp. 353–364, 2020.
- [18] C. Qi, F. Amato, M. Alhassoun, and G. D. Durgin, "Breaking the range limit of rfid localization: Phase-based positioning with tunneling tags," in *2019 IEEE International Conference on RFID (RFID)*. IEEE, 2019, pp. 1–8.
- [19] F. Amato, H. M. Torun, and G. D. Durgin, "Beyond the limits of classic backscattering communications: A quantum tunneling rfid tag," in *2017 IEEE International Conference on RFID (RFID)*. IEEE, 2017, pp. 20–25.
- [20] Y. Dia, H. Ribeiro, L. Oyhenart, E. Zaraket, J.-L. Lachaud, L. Fadel, V. Vigneras, C. Dejous, N. Carvalho, and S. Hemour, "Ultralow read sensitivity rfid sensor based on tunnel diode voltage-controlled oscillator," in *2023 IEEE 13th International Conference on RFID Technology and Applications (RFID-TA)*. IEEE, 2023, pp. 213–216.
- [21] J. A. Hagerty, F. B. Helmbrecht, W. H. McCalpin, R. Zane, and Z. B. Popovic, "Recycling ambient microwave energy with broadband rectenna arrays," *IEEE Transactions on Microwave Theory and Techniques*, vol. 52, no. 3, pp. 1014–1024, 2004.
- [22] R. Ludwig, *RF Circuit Design: Theory & Applications, 2/e*. Pearson Education India, 2000.
- [23] L.-G. Tran, H.-K. Cha, and W.-T. Park, "Rf power harvesting: a review on designing methodologies and applications," *Micro and Nano Systems Letters*, vol. 5, pp. 1–16, 2017.
- [24] S. Hemour, Y. Zhao, C. H. P. Lorenz, D. Houssameddine, Y. Gui, C.-M. Hu, and K. Wu, "Towards low-power high-efficiency rf and microwave energy harvesting," *IEEE transactions on microwave theory and techniques*, vol. 62, no. 4, pp. 965–976, 2014.
- [25] K. Niotaki, N. B. Carvalho, A. Georgiadis, X. Gu, S. Hemour, K. Wu, D. Matos, D. Belo, R. Pereira, R. Figueiredo *et al.*, "Rf energy harvesting and wireless power transfer for energy autonomous wireless devices and rfids," *IEEE Journal of Microwaves*, vol. 3, no. 2, pp. 763–782, 2023.
- [26] H. P. Paz, V. S. Silva, E. V. Cambero, H. X. Araújo, I. R. Casella, and C. E. Capovilla, "A survey on low power rf rectifiers efficiency for low cost energy harvesting applications," *AEU-International Journal of Electronics and Communications*, vol. 112, p. 152963, 2019.
- [27] X. Gu, W. Lin, S. Hemour, and K. Wu, "Readout distance enhancement of battery-free harmonic transponder," *IEEE Transactions on Microwave Theory and Techniques*, vol. 69, no. 7, pp. 3413–3424, 2021.
- [28] T. Taris, L. Fadel, L. Oyhenart, and V. Vigneras, "Cots-based modules for far-field radio frequency energy harvesting at 900mhz and 2.4 ghz," in *2013 IEEE 11th International New Circuits and Systems Conference (NEWCAS)*. IEEE, 2013, pp. 1–4.

- [29] J. Nicot and T. Taris, "Remote rf powering of ambient sensors," in *2016 IEEE International Conference on Electronics, Circuits and Systems (ICECS)*. IEEE, 2016, pp. 760–763.
- [30] J. Nicot, L. Fadel, and T. Taris, "An autonomous wireless sensor node based on hybrid rf solar energy harvesting," *Wireless Power Transfer*, vol. 2021, pp. 1–25, 2021.
- [31] R. Bergès, L. Fadel, L. Oyhenart, V. Vigneras, and T. Taris, "A dual band 915mhz/2.44 ghz rf energy harvester," in *2015 European Microwave Conference (EuMC)*. IEEE, 2015, pp. 307–310.
- [32] A. Abdollahi, N. Raghunathan, X. Han, B. Pattipati, B. Balasingam, K. Pattipati, Y. Bar-Shalom, and B. Card, "Battery health degradation and optimal life management," in *2015 IEEE AUTOTESTCON*. IEEE, 2015, pp. 146–151.
- [33] M. Uno and K. Tanaka, "Accelerated charge–discharge cycling test and cycle life prediction model for supercapacitors in alternative battery applications," *IEEE Transactions on Industrial Electronics*, vol. 59, no. 12, pp. 4704–4712, 2011.
- [34] S. Farzeen, G. Ren, and C. Chen, "An ultra-low power ring oscillator for passive uhf rfid transponders," in *2010 53rd IEEE International Midwest Symposium on Circuits and Systems*. IEEE, 2010, pp. 558–561.
- [35] M. Kumari and S. R. Hasan, "A new cmos implementation for miniaturized active rfid insect tag and vhf insect tracking," *IEEE Journal of Radio Frequency Identification*, vol. 4, no. 2, pp. 124–136, 2020.
- [36] T. N. Nguyen and J.-W. Lee, "Ultralow-power ku-band dual-feedback armstrong vco with a wide tuning range," *IEEE Transactions on Circuits and Systems II: Express Briefs*, vol. 59, no. 7, pp. 394–398, 2012.
- [37] Y.-S. Lin, C.-C. Wang, P.-W. Yu, J.-H. Lee, and S.-S. Lu, "Low-phase-noise 0.63-v, 1.7-mw, 11.55-ghz quadrature voltage controlled oscillator with intrinsic-tuned technique in 0.18- $\mu$ m complimentary metal oxide semi-conductor," *IET Microwaves, Antennas & Propagation*, vol. 6, no. 13, pp. 1437–1442, 2012.
- [38] K.-H. Lu, G.-L. Huang, and H.-Y. Chang, "A 17.5-dbm output power 11.2% dc-to-rf efficiency low phase noise cmos quadrature voltage-controlled oscillator," in *2018 IEEE/MTT-S International Microwave Symposium-IMS*. IEEE, 2018, pp. 1434–1437.
- [39] Z. Saheb and E. El-Masry, "An energy-efficient and ultra-low-voltage power oscillator in cmos 65 nm," *Analog Integrated Circuits and Signal Processing*, vol. 100, no. 1, pp. 149–156, 2019.
- [40] X. Gu, L. Grauwin, D. Dousset, S. Hemour, and K. Wu, "Dynamic ambient rf energy density measurements of montreal for battery-free iot sensor network planning," *IEEE Internet of Things Journal*, vol. 8, no. 17, pp. 13 209–13 221, 2021.
- [41] D. M. Pozar, *Microwave engineering*. John wiley & sons, 2011.
- [42] F. He, R. Ribas, C. Lahuec, and M. Jézéquel, "Discussion on the general oscillation startup condition and the barkhausen criterion," *Analog Integrated Circuits and Signal Processing*, vol. 59, pp. 215–221, 2009.
- [43] A. Bres, V. Guillerat, G. Ferré, and S. Hemour, "Towards battery-free wide area network with ultra-low voltage chirp spread spectrum modulation," in *2022 Wireless Power Week (WPW)*. IEEE, 2022, pp. 558–562.
- [44] C. H. P. Lorenz, S. Hemour, W. Li, Y. Xie, J. Gauthier, P. Fay, and K. Wu, "Breaking the efficiency barrier for ambient microwave power harvesting with heterojunction backward tunnel diodes," *IEEE Transactions on Microwave Theory and Techniques*, vol. 63, no. 12, pp. 4544–4555, 2015.
- [45] H. Ribeiro, S. Hemour, and N. Carvalho, "Ultralow power tunnel diode-based voltage controlled oscillator for the internet of things," *to be published*.
- [46] L. Fanori, A. Liscidini, and R. Castello, "Capacitive degeneration in lc-tank oscillator for dco fine-frequency tuning," *IEEE Journal of Solid-State Circuits*, vol. 45, no. 12, pp. 2737–2745, 2010.